PCCP

Accepted Manuscript

ROYAL SOCIETY OF CHEMISTRY

www.rsc.org/pccp

Electron spin relaxation in cryptochrome-based magnetoreception

Daniel R. Kattnig[1], Ilia A. Solov'yov[2,3] and P. J. Hore[1,*]

[1] Department of Chemistry, University of Oxford, Physical and Theoretical Chemistry Laboratory, OX1 3QZ, U.K.

[2] Department of Physics, Chemistry and Pharmacy, University of Southern Denmark, Campusvej 55, 5230 Odense M Denmark

[3] On leave from A. F. Ioffe Physical Technical Institute, Politechnicheskaya Str. 26, 194021 St.Petersburg, Russia.

*Corresponding author: peter.hore@chem.ox.ac.uk

ABSTRACT

The magnetic compass sense of migratory birds is thought to rely on magnetically sensitive radical pairs formed photochemically in cryptochrome proteins in the retina. An important requirement of this hypothesis is that electron spin relaxation is slow enough for the Earth's magnetic field to have a significant effect on the coherent spin dynamics of the radicals. It is generally assumed that evolutionary pressure has led to protection of the electron spins from irreversible loss of coherence in order that the underlying quantum dynamics can survive in a noisy biological environment. Here, we address this question for a structurally characterized model cryptochrome expected to share many properties with the putative avian receptor protein. To this end we combine all-atom molecular dynamics simulations, Bloch-Redfield relaxation theory and spin dynamics calculations to assess the effects of spin relaxation on the performance of the protein as a compass sensor. Both flavin-tryptophan and flavin-$Z^{\bullet}$ radical pairs are studied ($Z^{\bullet}$ is a radical with no hyperfine interactions). Relaxation is considered to arise from modulation of hyperfine interactions by librational motions of the radicals and fluctuations in certain dihedral angles. For *Arabidopsis thaliana* cryptochrome 1 (*At*Cry1) we find that spin relaxation implies optimal radical pair lifetimes of the order of microseconds, and that flavin-$Z^{\bullet}$ pairs are less affected by relaxation than flavin-tryptophan pairs. Our results also demonstrate that spin relaxation in isolated *At*Cry1 is incompatible with the long coherence times that have been postulated to explain the disruption of the avian magnetic compass sense by weak radiofrequency magnetic fields. We conclude that a cryptochrome sensor *in vivo* would have to differ dynamically, if not structurally, from isolated *At*Cry1. Our results clearly mark the limits of the current hypothesis and lead to a better understanding of the operation of radical pair magnetic sensors in noisy biological environments.

INTRODUCTION

Various animals, vertebrates and invertebrates, are capable of perceiving the intensity and/or direction of the Earth's magnetic field for the purposes of navigation and orientation. Although the compass magnetoreceptor has yet to be identified, a number of studies suggest a quantum-chemical mechanism relying on transient spin-correlated radical pairs, formed by photo-activation of the flavoprotein cryptochrome (for reviews, see [1-6]). Alternative — essentially classical — hypotheses have been proposed, the most prominent involving iron-containing magnetic nanoparticles [7-13]. None of these models can be regarded as definitely or exclusively established. In birds, for example, both mechanisms may co-exist [3, 14].

The radical pair hypothesis originates from an early suggestion by Schulten *et al*. [15]. Drawing on the known magnetic sensitivity of radical pair reactions *in vitro* [16-18], it was proposed that the coherent evolution of non-equilibrium spin states under the influence of anisotropic hyperfine interactions could form the basis of a magnetic direction sensor. In 2000, cryptochromes — blue-light photoreceptor proteins with a variety of functions and high sequence-homology with photolyases (DNA repair enzymes) [19] — were proposed as potential receptor molecules, located in the retina [20]. Sixteen years later, cryptochrome is still the only candidate chemical magnetoreceptor and evidence is accumulating in favour of the radical pair model and the cryptochrome hypothesis. We mention here a few, pertinent findings. (a) Cryptochrome 1a has been found in the avian retina, associated with the membrane discs in the outer segments of the UV/violet cones [21]. Expression levels of cytosolic cryptochromes are high in ganglion cells at times when birds perform magnetic orientation and the cells are neuronally active [22]. (b) Cryptochrome appears to be an essential element in the responses of fruit flies to weak magnetic fields [23]. (c) In some species the ability to sense magnetic fields is light-dependent and exhibits an action spectrum related to the optical absorption spectrum of the flavin cofactor in cryptochrome [24-26]. (d) Weak radiofrequency magnetic fields, including anthropogenic electromagnetic noise, have been reported to disrupt the ability of migratory birds to orient in the Earth's magnetic field[27-29]. (e) The yields of transient radicals in cryptochromes *in vitro* are magnetically sensitive [30]. The radical pair mechanism is currently the only physically plausible way in which these observations can be reconciled with biochemical effects of magnetic interactions (~100 neV mT^{-1}) that are more than six orders of magnitude weaker than the thermal energy ($k_B T$ = 27 meV at 310 K).

Magnetoreception by cryptochromes requires the formation of appropriate radical pairs. According to the prevalent model [5, 31-36], the process involves light activation of the fully oxidized state of the flavin adenine dinucleotide (FAD) cofactor, which triggers a cascade of rapid electron transfers along a highly conserved triad of tryptophan (W) residues (W400 (W_A), W377 (W_B), and W324 (W_C) in *Arabidopsis thaliana* (*At*.) cryptochrome 1, see Figure 1 and Scheme S1). In experiments on isolated proteins *in vitro*, this process typically gives rise to a primary radical pair comprising the flavosemiquinone radical, $FAD^{\bullet-}$, and $TrpH^{\bullet+}$, the oxidized form of the distal, solvent-exposed tryptophan residue, W_C [30]. Alternative electron transfer pathways exist [37], and different radical pairs may be formed on a millisecond timescale (e.g. by electron transfer from tyrosine residues [33]) if the Trp triad is disrupted [38], or (possibly) if external electron donors, e.g. ascorbic acid, are involved [39]. In any case, the charge separation reaction is fast, typically completed within 100 ps [40], and preserves the spin states of the precursor molecules, such that the radical pair is initially generated as an electronic singlet [41]. This non-equilibrium state represents a non-stationary coherent superposition

of the eigenstates of the spin Hamiltonian which evolves as a result of the anisotropic hyperfine interactions of the electron spins with nearby magnetic nuclei and the electron Zeeman interactions with an external magnetic field [42, 43]. The latter has the effect of modifying the energies of the singlet and triplet levels, thereby altering the rates of singlet-triplet interconversion. The magnetic field effect that is most relevant here, the so-called 'low field effect', is attributed to lifting degeneracies amongst the zero-field energy levels [44]. With a spin-selective recombination reaction occurring exclusively from the singlet state, the chemical reaction yields depend on the intensity and, for an immobile or slowly reorienting protein, the direction of an external magnetic field. Eventually, the primary radical pair is stabilized (independently of its spin state) by (de-)protonation to form a secondary pair ([$FADH^{\bullet}$ $Trp^{\bullet}$] in *At*Cry 1, on a microsecond timescale [30]). This form of the protein is thought to lead to the magnetic signalling state. (For an alternative, physical, model see [45].) No intrinsic magnetic sensitivity has been observed for this secondary radical pair. In insect cryptochromes, the microsecond proton transfer has not been observed and $FAD^{\bullet-}$, rather than $FADH^{\bullet}$, may give rise to the signalling state [35, 46]. An alternative proposal has the fully reduced form of FAD reacting with molecular oxygen to form a radical pair containing the superoxide radical, $O_2^{\cdot-}$ [26, 29, 47, 48]. Although this seems an improbable basis for a geomagnetic sensor [48], some of the results discussed below are transferable to this hypothesis.

In vitro studies have shown that for both cryptochrome and photolyase the quantum yield of the secondary radical pair is sensitive to the strength of an external magnetic field. At temperatures of 260–270 K, a 28 mT magnetic field elicited 10–20% changes in the reaction yield of the secondary pair [30]. In addition, a low field effect with inverted phase was observed for magnetic fields of 1–2 mT. These findings suggest that the proteins are, in principle, fit for purpose as chemical magnetoreceptors, in particular if conditions can be realized in which singlet-triplet dephasing and related spin relaxation mechanisms are sufficiently slow [30]. *In vitro* observations of chemical reactions responding to magnetic fields as weak as the Earth's (ca. 50 μT) are scarce. One of the few examples is the charge recombination of a radical pair in a carotenoid-porphyrin-fullerene model system which is affected by fields as weak as 39 μT [49]. To detect an anisotropic chemical response — a prerequisite for a compass sensor — fields of the order of 1 mT were required under otherwise similar conditions [49]. These measurements entailed cryogenic conditions to mitigate the effects of spin relaxation, which at room temperature effectively obliterate all coherences before the external magnetic field has an impact on the spin dynamics. A curious magnetic field effect on a sub-nanosecond component in the decay of photoexcited FAD in pigeon cryptochrome 1 has been reported [50]. This effect was observed at room temperature for field intensities in the range 45–285 μT. It is not clear whether the effect genuinely originates from spin evolution in a radical pair and, if it does, how the effect is transferred back to the fluorescent excited state of the FAD on a timescale faster than a nanosecond.

Thermal motions within the cryptochrome and, if relevant, rotational tumbling stochastically modulate the spin Hamiltonian parameters and thereby cause spin coherences and populations to relax towards thermal equilibrium. Such processes reduce the sensitivity to weak magnetic fields. Once the spin system is fully relaxed, the only possible effect of a weak magnetic field would be a negligible shift in the position of a chemical equilibrium or the rate constant of an activated chemical reaction.

In general, the response of a spin-correlated radical pair to a magnetic field of flux density *B* requires that $|\gamma_e| B\tau \ll 1$, where γ_e is the magnetogyric ratio of the electron and τ is the lifetime of the radical pair or of the spin-coherence, whichever is smaller. Ideally, the time taken for the coherence to dissipate should exceed the time required for the radical pair to react [2, 36]. In particular, spin relaxation must be slow enough to allow time for the magnetic field to induce additional coherent oscillations. Thus, in order to sense the Earth's magnetic field (ca. 50 μT), in which the electron Larmor frequency ($|\gamma_e| B/2\pi$) is approximately 1.4 MHz, coherence lifetimes of at least 100 ns are required [4]; optimal sensitivity is attained for $\tau \approx 1$ μs, i.e. long enough for one complete period of the Larmor precession. More stringent requirements on τ may result from the observed effects of low-amplitude radiofrequency magnetic fields (ca. 1 nT) on the ability of European robins to use their magnetic compass [27-29]. Based on the above relation, sensitivity to a 10 nT monochromatic oscillating magnetic field would require τ to be greater than about 600 μs.

It is currently unknown whether the coherence times attainable in cryptochromes in "wet, warm, and noisy" biological surroundings satisfy the above conditions (or whether the signals available from a radical pair sensor would be sufficient to elicit a physiological response to the geomagnetic field). Although 9 GHz electron paramagnetic resonance experiments on flavin-tryptophan radical pairs in cryptochromes suggest spin-relaxation times as long as 6 μs at 1 °C [32], this measurement does not readily generalize to physiological temperatures and Earth-strength fields.

Recently, several theoretical studies of the quantum spin dynamics of simple model radical pairs have stressed the importance of spin relaxation and have included it by means of a Lindblad master equation [51-56]. However, these approaches are phenomenological: they include neither a realistic description of the protein dynamics nor its coupling to the spin dynamics via appropriate magnetic interactions. Here, we attempt to overcome this limitation by employing all-atom molecular dynamics (MD) simulations to derive a realistic model of spin relaxation in radical pairs in an immobilized cryptochrome molecule. While many experimental and theoretical studies [20, 34, 39, 42-44, 57-62] have tested selected aspects of radical pair-based magnetoreception, spin relaxation and motion have not been addressed in detail, i.e. with realistic atomic-level motions and magnetic interactions.

METHODS AND MODELS

The model system

We focus on the spin relaxation of a radical pair embedded in an orientationally fixed cryptochrome molecule. As a model system we have chosen *At*Cry1 because its crystal structure [63] and photochemistry are known from detailed experimental [30] and theoretical studies [64-66]. Furthermore, this is the only cryptochrome for which magnetic field effects have been unequivocally demonstrated, albeit under non-physiological conditions [30]. Effects of weak magnetic fields on *A. thaliana* seedlings have also been discussed, but are controversial [67-69]. Neither the crystal structure nor the details of the photochemistry of any of the four avian cryptochromes are currently known [31], precluding their use at present in this type of study. We anticipate similar spin relaxation properties for members of the cryptochrome protein family when the following conditions are satisfied (structural similarities are discussed in Ref. [19]): (a) a high sequence homology, (b) a common overall fold, (c) a similar environment of the flavin isoalloxazine ring (including the distinctive U-shaped

conformation of the FAD, the Asp–Arg salt bridge in the isoalloxazine binding pocket, and the hydrogen bonding structure) and (d) a similar environment of the conserved tryptophan triad (including the distal Trp_C and its hydrogen-bonds with Met and Cys in a conserved motif).

Molecular dynamics simulations

MD simulations allow a detailed assessment of the protein motions that induce spin relaxation. We performed all-atom simulations for a modified version of the crystal structure of *At*Cry1 (PDB ID 1U3C [63]) containing the flavin radical, $FAD^{\bullet-}$, and the oxidized W324(H)$^{\bullet+}$ residue (Trp_C). Force-field parameters and atomic charges for the radicals were developed in a previous study [66]. Detailed information on the simulations is given in the Supporting Information. The protein was solvated in an aqueous solution of 50 mM NaCl. The combined system contained 113,455 atoms. After extensive equilibration, seven statistically independent MD trajectories, three spanning 300 ns and four covering 100 ns, were accumulated for the microcanonical ensemble at 300 K. The initial configuration of the system was identical in all simulations; stochastic behaviour emerged from the Langevin thermostat [70], as implemented in NAMD [71]. The protein motions were sampled at intervals of 0.5 or 5 ps. The accumulated trajectories cover 1.3 μs or 1,510,958 frames and occupy 140 GB of storage (without solvent). Some aspects of the choice of model are discussed in the following paragraphs.

We have assumed that the isoalloxazine ring of the FAD cofactor and the distal tryptophan, W_C, are ionized (see Figure 1). In principle, the electron transfer between W_B and W_C is reversible [30]. However, with a free energy difference between the radical pairs FAD-W_B and FAD-W_C of −0.38 eV [64], the back-electron transfer may not be significant during the lifetime of the primary pair. As a consequence, the reversibility of the electron transfer was neglected here. The aspartic acid residue D396 was modelled in its protonated form in agreement with the finding in Ref. [64] that the solvent-driven electron transfer outruns the protonation of $FAD^{\bullet-}$ by $W_A^{\bullet+}$.

In order to function as a compass sensor, the radical pair must be held in a well-defined orientation within the host organism and hence the protein must be immobilized and probably [58] (at least partly) aligned. While recent localization studies indicate that this may be achieved in the retina by anchoring the protein to the membrane discs in the outer segments of the ultraviolet/violet photoreceptor cones [21], the details of this immobilisation including the putative binding partner/anchor region remain opaque. To avoid introducing additional unsupported conjectures, we decided to model a globular protein solvated in aqueous NaCl (in a periodic box of dimensions 103 × 111 × 99 Å^3) and remove the overall rotational and translational motion of the protein *post factum*. Note that the photolyase homology region of cryptochrome 1 does not exhibit obvious anchoring motifs and that the driving force controlling the fast charge separation along the tryptophan triad results from differential solvation [64, 72]. Both points suggest that the immediate surroundings of the photolyase homology domain in an actual compass sensor cannot differ seriously from the assumptions imposed here; otherwise the charge separation would probably be impeded. In order to calculate the relaxation parameters of the compass sensor, we aligned the protein backbone at each MD time-step by a rigid body rotation/translation such that the positions of the α-carbon atoms matched (in a least-squares sense) the orientation of the reference structure, the coordinate system of which was aligned with the eigenvectors of its inertia tensor. In this process, the rotational motion (correlation time about different axes: 11–13 ns) and translational diffusion (diffusion coefficient:

0.46 ± 0.02 Å^2 ns^{-1}) of the protein as a whole were removed. Note that this approach does not remove motions internal to the protein, e.g. those of backbone segments, and thus mimics the scenario of immobilization without undue increase in rigidity. Spin relaxation due to rotational tumbling of the photoreceptor within an ordering potential has been discussed in detail in Ref. [58]. Note, furthermore, that in order to function as a radical pair-based magnetoreceptor even modest uniaxial molecular alignment of the protein would suffice [58-60]. For the sake of lucidity, we do not discuss static disorder here. However, it is to be understood that this point can always be addressed having first calculated the primary magnetic field effects including the relaxation pathways within the protein.

Magnetic interactions and their stochastic modulation

Spin relaxation results from stochastic fluctuations of local magnetic fields. In radicals, these fluctuating fields can result from modulations of spin Hamiltonian parameters such as those of the isotropic or anisotropic hyperfine interactions. A qualitative picture of the latter is as follows. The nuclear magnetic moments produce a local magnetic field component experienced by the electron spin. A molecular reorientation changes the relative positions of the spins in space, but leaves the spin-quantisation axes (initially) unaffected. As a consequence, the local field sensed by the electron is altered, and in the course of many random reorientations this results in dephasing and induces spin transitions.

There are several sources of stochastic modulation of the spin Hamiltonian parameters. Here, we consider two dominant modes. (a) Modulation of anisotropic hyperfine interactions by librations, i.e. small-angle reorientations of the aromatic rings of the radicals within the protein. (b) Modulation of hyperfine coupling parameters by fluctuations in the dihedral angle that determines the orientation of the aromatic ring with respect to the remainder of the radical. Changes in this angle have a particularly strong impact on the isotropic coupling constants of the β-methylene hydrogens in both radicals for which a Heller-McConnell-type dependence is typical [73]. Fluctuations of the inter-radical distance, and (to a lesser extent) the relative orientation of the radicals in the protein-fixed frame, modulate the mutual dipolar coupling of the two radical centres. This relaxation pathway is significantly slower than the processes mentioned above and is neglected here. With the above-mentioned motions accounted for, the dynamics of the protein can be comprehensively described by just 8 parameters, from which the spin relaxation properties can be calculated: 3 Euler angles are necessary to specify the orientation of each of the radicals, and 2 dihedral angles specify the internal structure of the radicals, as mentioned above. In principle, additional internal degrees of freedom could be included in the analysis, the most obvious candidates being methyl group rotation [74] and the butterfly motion of the flavin isoalloxazine ring system [75]. The latter is relevant to the ultrafast dynamics of the excited states of flavins and determines important properties such as ionization potentials [75, 76]. However, it turns out that these motions give rise to comparatively small variations of the hyperfine parameters and, above all, are too fast to appreciably influence the spin relaxation [75]. The hyperfine interactions of the electron spins of the radical pair and the nuclear spins of atoms in the environment — in particular hydrogen atoms in the surrounding water molecules — offer another pathway for the loss of coherence. This effect, which has been considered in Refs [77, 78], gives rise to relaxation times of the order of milliseconds, which is negligibly slow compared to the processes discussed above.

We performed density functional calculations (Gaussian 09, Revision A.02 [79]; ub3lyp/6-311g(d,p) // ub3lyp/epr-ii) on model compounds to relate the internal structure as defined by the relevant dihedral angles to the hyperfine coupling parameters. *N*-acetyl-*N*′-methyl-L-α-tryptophanamide (dihedral angle: Cα-Cβ-C3-C3a; see Figure S2) and riboflavin (dihedral angle: C10a-N10-C1′-C2′) were used as models of the tryptophan and FAD radicals, respectively. The data reveal (see Figure S3) that the mobility of the aromatic ring relative to the rest of the side-chain induces strong modulation of the hyperfine tensors of the Trp radical. In particular the isotropic hyperfine coupling constants of the two β-methylene protons show a pronounced torsional dependence. While the rotamers are sufficiently constrained as not to sample the entire torsional configuration space, the average dihedral angle lies within the region of maximum gradient of one of the two coupling constants with respect to the angle, such that an efficient spin relaxation channel is anticipated. On the contrary, the hyperfine couplings of the C1′ protons in the flavin radical are only weakly dependent on the dihedral angle. Although not discussed in detail here, the spin-dynamics simulations described below account for variations in all hyperfine parameters — principal values and principal axes — caused by the torsional motion.

Spin dynamics

We have calculated the impact of spin relaxation on the anisotropy of the yield of the product formed from the singlet state of the radical pair subject to an Earth-strength (50 μT) magnetic field. The Bloch-Redfield formalism [80, 81] was employed, because it allows a master equation to be derived from the microscopic description of the bath (in terms of the 8 variables discussed above) and the known system-environment interaction operators (given by the spin Hamiltonian and the conformational dependence of the hyperfine terms). The approach starts from a combined system-environment perspective, and derives a perturbative master equation for the (spin) system, under the assumption of weak system-environment coupling. Details are given in the Supporting Information. Terms in the relaxation superoperator are proportional to spectral densities, $J(\omega)$, which are one-sided Fourier transforms of covariance functions of the form:

$$g_{f,h}(t) = \left\langle \left(f(0) - \langle f \rangle\right)\left(h(t) - \langle h \rangle\right) \right\rangle \qquad (1)$$

where *f* and *h* denote interaction parameters of the spin Hamiltonian (e.g. certain components of hyperfine interaction tensors) and angled brackets denote time averages (we assume stationary ergodic processes). In contrast to the Lindblad master equation, the dissipation processes and rates are obtained directly from the properties of the environment, i.e. the correlation functions of the effective parameters of the spin Hamiltonian. In general, the motions observed here with correlation times in the range of picoseconds to tens of nanoseconds and can be well treated.

RESULTS

Librational motions

The insets in Figures 2a and 2b illustrate the librational motions of $FAD^{\bullet-}$ and $W_C^{\bullet+}$, respectively, by means of typical trajectories of the radical-fixed coordinate axes in the protein-fixed frame. The $FAD^{\bullet-}$ is held firmly in place, undergoing librations of, on average, only 5.8°, 4.7°, and 5.8° about the molecular *x*, *y*, and *z*-axes, respectively. The orientation of $W_C^{\bullet+}$ is considerably more variable, with

average libration angles of 11.0° (*x*), 12.4° (*y*) and 12.2° (*z*). The distributions of libration angles are well approximated by Rayleigh distributions [82] for all three axes of both radicals[82]. In general, spin relaxation is not just a function of the amplitudes of the magnetic interactions but also critically depends on the timescale of the underlying motion. Some of the pertinent temporal aspects of the librational motion can be assessed from the auto-covariance functions of $P_2(\cos\theta) = ½(3\cos^2\theta - 1)$, where θ is the angle between a particular molecular axis and its average orientation in the protein-fixed frame (see eqn. (1)). This function transforms under rotation in the same way as the anisotropic parts of the hyperfine interactions. Note, however, that here the zero-order components of the interaction tensors also vary with the fluctuation in the internal degrees of freedom. The auto-covariance functions (Figures 2a and b) expose a fast decay component, which is not resolved with the minimum sampling time of the simulations (500 fs). These unresolved components are much too fast to cause spin relaxation in weak magnetic fields and can be unconditionally ignored. In fact, it is the zero-frequency and low-frequency Fourier components of the covariance functions that determine the relaxation operator. The more gradual decay of the covariance function of $FAD^{\bullet-}$ compared to that of $W_C^{\bullet+}$ is the result of its lower mobility. In summary, the librational motions of $W_C^{\bullet+}$ are large in amplitude and relatively fast, whereas those of $FAD^{\bullet-}$ have a lower amplitude and are slower. In both cases, relatively efficient spin relaxation can be anticipated.

Fluctuations of the side-chain dihedral angles

The dihedral angle (see Figure 1 and Figure S2) that defines the orientation of the aromatic ring in $W_C^{\bullet+}$ with respect to the remainder of the residue is more variable than the corresponding angle in $FAD^{\bullet-}$. In both cases, the dihedral angles are approximately normally distributed with average values and standard deviations: 94.7° ± 5.4° for $FAD^{\bullet-}$ and −74.2° ± 11.3° for $W_C^{\bullet+}$ (see the inset in Figure 2c). In general, the greater manoeuvrability of $W_C^{\bullet+}$ is not surprising in view of its location within a loop region (α11/12) in the protein, in contrast to the enclosed, hydrogen-bonded environment of the flavin part of the $FAD^{\bullet-}$ [19]. For the latter, the torsional oscillations are further restricted by an intramolecular hydrogen-bond involving the ribityl chain. The torsional correlation functions, i.e. the auto-covariance functions of $\cos\theta$, with θ denoting the dihedral angle, decayed to 35% ($FAD^{\bullet-}$) and 17% ($W_C^{\bullet+}$) of their initial values after 500 fs; again these fast decays do not lead to significant spin relaxation. Evidently a large fraction of the motion can be attributed to local vibrational modes. As a result of the strong dependence of the hyperfine parameters on the dihedral angle, efficient relaxation can be expected for $W_C^{\bullet+}$. Slower relaxation is anticipated for $FAD^{\bullet-}$: the slower decay of the covariance function is outweighed by the considerably weaker dependence of its hyperfine parameters on the dihedral angle.

Motionally averaged hyperfine interactions

Figure 3 shows the average hyperfine interactions over the course of the MD trajectories and the associated standard deviations. For $FAD^{\bullet-}$, the hyperfine interactions are dominated by the two nitrogen atoms in the central ring (N5 and N10) and, to a lesser extent, by H1, the two β-protons and the three methyl protons at C8α. Only the N5 and N10 positions show marked variations of the hyperfine terms as a result of the radical motion. A more detailed analysis (Figure S4) reveals that the variations in the hyperfine terms are predominantly caused by librations. In $W_C^{\bullet+}$, the spin density is more evenly distributed over the ring system. The β-protons and all nuclei in the aromatic ring system except H5 and H7 have strong time-averaged hyperfine interactions. The standard deviations of the hyperfine coupling constants result predominantly from the modulation of the dihedral angle,

in particular for the β-methylene protons. For the atoms H1, N1 and H2, librations contribute significantly to the hyperfine fluctuations; for other positions the librations are of minor importance. The motionally-averaged hyperfine coupling tensors are summarized in Tables S1 and S2 in the Supporting Information.

Spectral densities

In Bloch-Redfield theory, the spin-relaxation rates are proportional to spectral density functions evaluated at the frequencies corresponding to differences in the energy eigenvalues of the time-independent part of the spin Hamiltonian (see Supporting Information). The efficacy of different relaxation processes can be assessed by means of the values of the relevant spectral densities at zero frequency, $J(0)$ (see eqn. 7 in the Supporting Information). Table 1 gives some of the important spectral densities as their reciprocals, $J(0)^{-1}$, which we henceforth treat as typical relaxation times. Note that in the process of assembling the relaxation operator, the spectral densities are scaled by a term bilinear in matrix elements of spin operators. For this reason and the fact that the spectral densities are smaller for non-zero frequencies, the actual relaxation times are to be expected longer than $J(0)^{-1}$ by up to about an order of magnitude.

It is apparent from Table 1 that the fluctuations in hyperfine fields resulting from internal motions within the protein can induce efficient spin relaxation in both radicals. For $FAD^{\bullet-}$, the relaxation process is dominated by the auto-correlation contribution from N5 ($J(0)^{-1} \approx 70$ ns) and its cross-relaxation with N10 and H6. The second fastest auto-relaxation comes from N10 as expected from the motion-induced variations in the hyperfine interactions illustrated in Figure 3. Thus, the relaxation efficiency follows the order N5 > N10 > H6, with the remaining nuclei only contributing marginally to the overall relaxation operator. For $W_C^{\bullet+}$, the most efficient relaxation pathways result from the auto- and cross-terms for the methylene protons (fastest contribution: Hβ1, $J(0)^{-1} = 76$ ns), which are strongly affected by the fluctuations in the Cα-Cβ-C3-C3a-dihedral angle. Cross-relaxation with Hβ1 is the most efficient pathway for the aromatic protons. In summary, based on $J(0)^{-1}$, we find the following approximate ordering by relaxation efficiency: Hβ1 > Hβ2 > H1 > H4 > N1 > H6 > H7 >> H5. With typical relaxation times of the order of 100 ns and longer, the hyperfine-induced relaxation is expected to be non-negligible during the ca. 1 μs lifetime of the radical pair.

We mention in passing that fluctuations in the inter-radical distance modulate the dipolar coupling constant, which is proportional to the inverse cube of the radical separation, leading to relaxation. However, we find that $J(0)^{-1}$ is more than 10 μs, justifying our neglect of this interaction.

Spin relaxation in [FAD$^{\bullet-}$ Z$^{\bullet}$]

Theoretical and experimental studies have hinted at the possibility of a magnetically-sensitive radical pair in which a cryptochrome-bound $FAD^{\bullet-}$ is paired with a radical devoid of hyperfine interactions (here denoted $Z^{\bullet}$). For [$FAD^{\bullet-}$ $Z^{\bullet}$], a "Zeeman resonance" is predicted (and has been reported [29]), large low-field effects result [83], and the anisotropy of the magnetic field effect is expected to be larger by at least an order of magnitude than for [$FAD^{\bullet-}$ $W_C^{\bullet+}$] [39]. The ascorbyl radical [39], the superoxide radical, and dioxygen [29, 47] have been suggested as candidate $Z^{\bullet}$ radicals. However, the last two cannot be reconciled with their physical properties [48, 84] and the first contains a single (weakly) hyperfine-coupled proton [39]. Irrespective of the biochemical reality, the [$FAD^{\bullet-}$ $Z^{\bullet}$] model is valuable in assessing the contribution of the $FAD^{\bullet-}$ moiety to the compound relaxation pathways in

[$FAD^{\bullet-}$ $W_C^{\bullet+}$]. We have evaluated the singlet yield and its anisotropy for an Earth-strength magnetic field (50 μT) using singlet and triplet reaction rate constant ($k_S = k_T = 10^6\ s^{-1}$) chosen to give a lifetime (1 μs) roughly consistent with the radical decay rates observed experimentally [30]. Spin relaxation was included for $FAD^{\bullet-}$ but not for $Z^{\bullet}$. The anisotropic components of the singlet yield are illustrated in Figure 4 and Figure S5 for a series of radical pairs differing in the number and the identity of the nuclear spins included in the model of the $FAD^{\bullet-}$ radical. We characterize the spin dynamics in terms of two parameters, the mean singlet yield, $\bar{\Phi}_S$ and the singlet yield anisotropy, Γ. $\bar{\Phi}_S$ is the probability that the radical pair recombines via the singlet reaction channel, averaged over all orientations of the magnetic field with respect to the radical pair. Γ is defined as $\{\max(\Phi_S) - \min(\Phi_S)\}/\bar{\Phi}_S$, the difference between the maximum and minimum values of the anisotropic singlet yield divided by $\bar{\Phi}_S$. We also refer to Γ as the "compass sensitivity".

Whether relaxation is included or not, the anisotropic part of the singlet yield for [$FAD^{\bullet-}$ $Z^{\bullet}$] was found to be dominated by the two nitrogen atoms, N5 and N10, which are characterized by near-axial hyperfine interactions with almost collinear principal axes. The singlet yield anisotropies, with and without relaxation, have a similar shape that closely resembles the axially symmetric, second order spherical harmonic $Y_2^0 \propto 3\cos^2\theta - 1$ (Figure 4), although there are small contributions from higher order terms. In the absence of relaxation, the mean singlet yield and the anisotropy are $\bar{\Phi}_S$ = 0.407 and Γ = 0.517 for a radical pair containing only N5 and N10. Adding additional spins from the set Hβ1, Hβ2, H6 increases the anisotropy (on average, to Γ = 0.59). Only after including the 3 methyl protons at C8α to form an eight-nucleus radical pair, i.e. N5, N10, Hβ1, Hβ2, H6, and 3 x H8α, did Γ fall below that found for the N5, N10 case. At Γ = 0.502, however, the anisotropy is still high and could form the basis of a sensitive magnetoreceptor. This observation is in agreement a previous study [39].

When hyperfine-induced relaxation is included, using the motional correlation functions obtained from the MD trajectories, the singlet yield anisotropy is reduced. Without cross-relaxation terms we observe the following. For a radical pair comprising the two nitrogen atoms in $FAD^{\bullet-}$, Γ decreases by just 11%. With any combination of the ^1H hyperfine interactions added to the nitrogens, Γ is further reduced, but by no more than about 19%. This also holds for the eight-nucleus radical pair discussed above (Γ = 0.407). Cross-relaxation arising from hyperfine terms associated with different nuclei is relatively unimportant. Taking these additional relaxation pathways into account, the proton-containing radical pairs suffer a relaxation-induced reduction in Γ of 17 ± 1% with respect to the corresponding non-relaxing systems. In summary, hyperfine-induced relaxation preserves the potential sensitivity of [$FAD^{\bullet-}$ $Z^{\bullet}$] as a compass sensor. When the lifetime is 1 μs, Γ (and $\bar{\Phi}_S$) are not strongly attenuated and the shape of the anisotropy is relatively invariant for all radical pairs studied.

Spin relaxation in [$FAD^{\bullet-}$ $W_C^{\bullet+}$]

The anisotropy patterns for [$FAD^{\bullet-}$ $W_C^{\bullet+}$] are more diverse and the sensitivity to the direction of the magnetic field drastically reduced compared to [$FAD^{\bullet-}$ $Z^{\bullet}$]. This is a consequence of having several nuclei in $W_C^{\bullet+}$ with comparable hyperfine coupling constants and no approximate symmetry axis as there is in $FAD^{\bullet-}$. Figure 5 and Figure S6 illustrate the effect of including additional nuclei in the reference model containing only the two dominant $FAD^{\bullet-}$ nitrogens. For a 50 μT magnetic field and k_S

= k_T = 10^6 s^{-1} as above, the addition of, for example, N1 in $W_C^{\bullet+}$ reduced the anisotropy to Γ = 0.21, a value smaller by a factor of nearly 2.5 compared to the reference model with no hyperfine interactions in the second radical. H2 (Γ = 0.053), H6 (Γ = 0.050) and H1 (Γ = 0.080) are particularly detrimental to the compass sensitivity. Moreover, sequential addition of nuclei to $W_C^{\bullet+}$ in [$FAD^{\bullet-}$ $W_C^{\bullet+}$] leads to a stepwise reduction in Γ. For a model comprising N5 and N10 in $FAD^{\bullet-}$ and H1, H2, H4, H6, Hβ1, Hβ2, and N1 in $W_C^{\bullet+}$ (9 nuclei in total), Γ = 0.017 is 28 times smaller than for [$FAD^{\bullet-}$ $Z^{\bullet}$]. For the same model, $\overline{F}_S$ = 0.26 which is close to the fully relaxed value of 0.25.

Spin relaxation is faster in [$FAD^{\bullet-}$ $W_C^{\bullet+}$] than in [$FAD^{\bullet-}$ $Z^{\bullet}$] because additional, efficient relaxation pathways are available – in particular those associated with Hβ1, Hβ2, and H1 in $W_C^{\bullet+}$. Figure 5 gives some representative examples. Retaining only N5 and N10 in $FAD^{\bullet-}$ as above, the addition of Hβ1 and Hβ2 to $W_C^{\bullet+}$ reduces Γ by 38.0% (excluding cross-relaxation). With H1 as well, the reduction is 52.5%. Subsequent inclusion of any of the other nuclei (e.g. N1, H5, and H2) does not strongly alter the percentage reduction, which approximates to 50% for these larger spin systems. Note however that Γ for these larger systems is small even without relaxation. For example, with Hβ1, Hβ2, H1, N1, H5 and H2 added to the two-nitrogen FAD-model, the anisotropy of the relaxing radical pair is very small (Γ = 0.0080) largely because the relaxation-free value is only about twice this size.

We have also tried to assess the relaxation behaviour in more realistic radical pairs. With 5 nuclei in the FAD radical (N5, N10, Hβ1, Hβ2, H6), we find reductions of 34.7%, 60.3%, and 80.0% when extending the $W_C^{\bullet+}$ spin system to comprise 2, 3, and 6 additional nuclear spins (Hβ1, Hβ2, H1, N1, H2 and H4, added in the order given). In contrast to the simpler system described above (in which $FAD^{\bullet-}$ contains only N5 and N10), the reduction in Γ does not level off in this series of calculations; enlarging the system is always accompanied by a larger percentage loss of sensitivity. For the largest system, the anisotropy of the magnetic field effect has been practically eradicated and amounts to only Γ = 0.00094 (with $\overline{F}_S$ = 0.257). This corresponds to a reduction by a factor of 500 with respect to the corresponding [$FAD^{\bullet-}$ $Z^{\bullet}$] case.

Close inspection of data compiled in the Supporting Information reveals furthermore that cross-relaxation effects among different nuclei within $W_C^{\bullet+}$ are less significant than for $FAD^{\bullet-}$. The singlet anisotropy of the relaxing systems is typically reduced by approximately 1% when the cross-terms are taken into account. For example, for the (N5, N10, Hβ1, Hβ2, H6) + (Hβ1, Hβ2, H1) system Γ = 0.0287 and 0.0281 without and with cross-relaxation, respectively. It is further interesting to note that in the presence of $W_C^{\bullet+}$, the singlet yield anisotropy drops when the number of nuclear spins of the $FAD^{\bullet-}$-subsystem is increased, i.e. the system becomes less robust to the presence of nuclear spins other than N5 and N10.

In summary, [$FAD^{\bullet-}$ $W_C^{\bullet+}$] lacks many of the advantageous properties of [$FAD^{\bullet-}$ $Z^{\bullet}$]. The magnetic field effects on the latter are dominated by the $FAD^{\bullet-}$ N5 and N10 hyperfine interactions and the spin relaxation they cause. The approximate axial symmetry of the hyperfine fields in $FAD^{\bullet-}$ is substantially reduced by the much less symmetric anisotropic hyperfine interactions in $W_C^{\bullet+}$, an effect that results in a much smaller Γ even though the pertinent spectral densities for $FAD^{\bullet-}$ and $W_C^{\bullet+}$ are of comparable size. The lack of an approximate symmetry axis in [$FAD^{\bullet-}$ $W_C^{\bullet+}$] also manifests

itself in the multitude of shapes exhibited by the singlet yield anisotropy (Figure 5), depending on which nuclei are included. Furthermore, Γ decreases strongly with the size of the spin system. For a lifetime of 1 μs, a singlet anisotropy of only $\Gamma \approx 0.001$ is predicted for the most realistic spin system studied here. It is difficult to know whether such a small magnetic field effect could form the basis of a viable compass sensor.

Spin relaxation in radical pairs of varying lifetime

The effect that spin relaxation has on a radical pair depends strongly on its lifetime in relation to the lifetime of the spin coherence. Given the diversity of relaxation pathways and with relaxation rates spanning multiple timescales, a single relaxation time cannot adequately characterize the behaviour of the systems studied here. The overall effects of relaxation can best be discerned through the dependence of quantities such as Γ and $\overline{F}_S$ on the radical pair lifetime. For the above simulations, a lifetime of 1 μs was assumed, guided by experimental findings [30]. However, much longer timescales are possible, at least in principle, especially in the context of the reported disorientation of European robins by very weak radiofrequency magnetic fields [27-29]. Such long lifetimes are the focus of this section.

For a series of model radicals, Figure 6 and Figure S7 show the lifetime-dependence of Γ for $[FAD^{\bullet-}\ Z^{\bullet}]$ and $[FAD^{\bullet-}\ W_C^{\bullet+}]$. In the latter case, the relaxation of both radicals (Figure 6) or only that of $W_C^{\bullet+}$ (Figure S7) is included. As shown by the positions of the maxima in Figure 6, the optimal directional sensitivity is obtained for lifetimes of the order of 1 μs. This is true for all the spin systems studied, with the optimum for $[FAD^{\bullet-}\ Z^{\bullet}]$ occurring at slightly shorter lifetimes than for $[FAD^{\bullet-}\ W_C^{\bullet+}]$. In both cases, the sensitivity is strongly attenuated for lifetimes in excess of 10 μs. For example, when the $FAD^{\bullet-}$ contains two nitrogens and three protons, Γ is approximately 2.3 times smaller than its maximum value if the lifetime is prolonged to 10 μs. For a lifetime of 100 μs, the attenuation is roughly 15-fold. This agrees with the failure to observe magnetic sensitivity for the (de-)protonated secondary FAD-Trp radical pair in cryptochrome, which has a lifetime of about 100 μs [30]. Our calculations also confirm the previously raised conjecture that the experimentally observed lifetime of ca. 1 μs seems to offer the best compromise between allowing enough time for a significant magnetic field effect to develop but not too much time for spin relaxation [34]. Consistent with this, for short lifetimes Γ is generally found to match that of the corresponding non-relaxing system.

DISCUSSION

We have explored the effects of spin relaxation on the directional sensitivity of a cryptochrome-based compass system operating via the radical pair mechanism. Spin relaxation has not previously been examined with reference to the microscopic details of the molecular motions and magnetic interactions responsible for the relaxation. Here we have tackled this question using all-atom molecular dynamics simulations in combination with spin dynamics calculations based on the Bloch-Redfield approach. Unlike the Lindblad formalism [51-56], this methodology allowed us to derive realistic estimates of the relaxation rates based on the intrinsic properties of the cryptochrome host. We have focused on spin relaxation resulting from stochastic motion of the radicals in the primary, charge-separated state comprising the anion radical of the FAD cofactor and either the cation radical of the distal tryptophan component of the conserved Trp-triad or an unknown (but previously

predicted [29, 49]) radical ($Z^{\bullet}$) lacking significant electron-nuclear hyperfine interactions. According to the current state of knowledge, these transient radical pairs are the most likely basis of the avian compass sensor.

We have focused on hyperfine-induced relaxation brought about by librational motions of the aromatic cores of the radicals and by fluctuations in certain dihedral angles. For both $FAD^{\bullet-}$ and $W_C^{\bullet+}$, efficient hyperfine-induced relaxation pathways exist, characterized by inverse spectral densities as small as ~100 ns. In all the cases considered here, hyperfine-induced relaxation was found to decrease the compass sensitivity relative to the corresponding non-relaxing reference. In $W_C^{\bullet+}$, efficient relaxation comes from the β-methylene protons, whose hyperfine interactions are predominantly modulated by fluctuations of the dihedral angle that determines the position of the indole ring relative to the remainder of the tryptophan side-chain. In $FAD^{\bullet-}$, librational motions induce effective relaxation by modulating the hyperfine interactions of N5 and N10. Although the local magnetic field fluctuations are of smaller amplitude in $FAD^{\bullet-}$, its more sluggish motion results in relaxation rates similar to $W_C^{\bullet+}$. Despite its fast spin relaxation pathways, the $FAD^{\bullet-}$ radical is surprisingly immune to spin relaxation when combined with a radical partner devoid of magnetic nuclei (the [$FAD^{\bullet-}$ $Z^{\bullet}$] radical pair). This configuration is characterized by high intrinsic directional sensitivity, largely due to the N5 and N10 nitrogens, which is hardly affected by the presence of additional hyperfine interactions. For a lifetime of 1 μs, spin relaxation causes a reduction in the directional sensitivity of less than 20%. For a realistic spin system, a 41% change in the singlet yield upon reorienting the magnetic field is predicted. When $FAD^{\bullet-}$ is paired with $W_C^{\bullet+}$ instead of $Z^{\bullet}$, many of these favourable properties are lost. The compass sensitivity is strongly reduced due to the unfavorably aligned hyperfine interactions in $W_C^{\bullet+}$ and a higher motional susceptibility. As a consequence, for the largest combined system considered here (11 nuclear spins), the singlet yield anisotropy is reduced to 0.1% for a lifetime of 1 μs. We anticipate, therefore, that it may be challenging to detect anisotropic magnetic field effects for [$FAD^{\bullet-}$ $W_C^{\bullet+}$] in cryptochromes or photolyases *in vitro*. Given that a [$FAD^{\bullet-}$ $Z^{\bullet}$] species can deliver much stronger directional information than the 'conventional' [$FAD^{\bullet-}$ $W_C^{\bullet+}$] radical pair, one can speculate whether Nature has found a way to pair the $FAD^{\bullet-}$ in cryptochrome with a radical that has fewer and smaller hyperfine interactions than does $TrpH^{\bullet+}$. We suggest that further consideration of this possibility may help identify the actual magnetic compass sensor.

For model radical pair systems subject to hyperfine-induced spin relaxation, the maximum compass sensitivity was found for lifetimes close to 1 μs for both [$FAD^{\bullet-}$ $W_C^{\bullet+}$] and [$FAD^{\bullet-}$ $Z^{\bullet}$]. Longer lived radical pairs suffer a marked loss of sensitivity; for a lifetime of 100 μs the signal is reduced by a factor of 10–20. It is interesting to note that lifetimes of the primary radical pair of the order of a microsecond have indeed been found in experimental studies *in vitro* [30]. We speculate that evolutionary pressure may have led to radical pair lifetimes that are optimized to yield maximal sensitivity in the presence of unavoidable spin relaxation processes. In view of our findings, we conclude that hyperfine-induced spin relaxation, while reducing the compass sensitivity, does not fundamentally impede the ability of cryptochromes to respond to the direction of the Earth's magnetic field *in vivo*.

One of the unknown aspects of the radical pair hypothesis is how large the fundamental response needs to be for a viable magnetoreceptor. We presume that the primary magnetic field effect *in vivo*

would have to be amplified and that this could compensate to some extent for any losses in sensitivity that arise from spin relaxation [85]. The alternative would be a sensor with substantially slower spin relaxation than has been calculated here. This would allow radical pair lifetimes to exceed a few microseconds which might have the advantages of a more precise compass bearing as well as helping to understand the apparent disorientation of European robins exposed to very weak radiofrequency fields [27-29, 78].

Arguments can be adduced to support the notion that spin relaxation could be slower *in vivo* and slower in *avian* cryptochromes. (a) Our calculations have been performed for an isolated cryptochrome; the internal dynamics could be quite different for the same molecule interacting with ligands and signalling partners and binding to whatever cellular structures are responsible for its immobilization and alignment in an avian magnetoreceptor. Such interactions could make the protein more rigid and/or constrain the slow, large scale 'breathing' modes that are particularly efficient at inducing relaxation. (b) The dynamics of the radicals in an avian magnetoreceptor cryptochrome may have evolved to be very different from those in homologous proteins that do not have a magnetic sensing function. Although there have been reports of cryptochrome-dependent magnetic field effects on plants and insects,[23, 67, 68, 86-91] these studies do not prove that the magnetically sensitive entity is cryptochrome. Also, one cannot infer from such observations that evolution has provided plants and insects with a sensitive magnetic direction sensor or that these organisms exploit the Earth's magnetic field to orient or navigate. The magnetic responses reported for plants and birds may have no functional relevance. By contrast, it is clear that birds have a magnetic compass and use it to orient themselves during migration. With the currently available evidence, one cannot be sure that the *Arabidopsis* cryptochrome studied here has similar behaviour to whichever of the four avian cryptochromes is involved in magnetoreception.

ACKNOWLEDGEMENTS

We thank the University of Oxford Advanced Research Computing (ARC) facility (http://dx.doi.org/10.5281/zenodo.22558) for generous allocation of CPU time, the Texas Advanced Computing Center (TACC) at the University of Texas at Austin, for providing supercomputer time on Stampede through the Extreme Science and Engineering Discovery Environment (XSEDE) Grant XSEDE MCB-120160, and the DeiC National HPC Center, SDU. IAS is grateful for financial support from the Lundbeck Foundation and the Russian Scientific Foundation (Grant No. 14-12-00342). PJH is grateful to the following for financial support: the European Research Council (under the European Union's 7th Framework Programme, FP7/2007-2013/ERC grant agreement no. 340451) and the Air Force Office of Scientific Research (Air Force Materiel Command, USAF award no. FA9550-14-1-0095).

REFERENCES

1. R. Wiltschko and W. Wiltschko, *Biosensors*, 2014, 4, 221-242.
2. T. Ritz, *Procedia Chem*, 2011, 3, 262-275.
3. H. Mouritsen and P. J. Hore, *Curr. Opin. Neurobiol.*, 2012, 22, 343-352.
4. I. A. Solov'yov, T. Ritz, K. Schulten and P. J. Hore, in *Quantum Effects in Biology*, eds. M. Mohseni, Y. Omar, G. S. Engel and M. B. Plenio, Cambridge University Press, Cambridge, 2014, DOI: Book_Doi 10.1017/Cbo9780511863189, pp. 218-236.
5. E. W. Evans, C. A. Dodson, K. Maeda, T. Biskup, C. J. Wedge and C. R. Timmel, *Interface Focus*, 2013, 3, 20130037.
6. M. Liedvogel and H. Mouritsen, *J. R. Soc. Interface*, 2010, 7, S147-S162.
7. H. Cadiou and P. A. McNaughton, *J. R. Soc. Interface*, 2010, 7, S193-S205.
8. C. D. Treiber, M. C. Salzer, J. Riegler, N. Edelman, C. Sugar, M. Breuss, P. Pichler, H. Cadiou, M. Saunders, M. Lythgoe, J. Shaw and D. A. Keays, *Nature*, 2012, 484, 367-371.
9. S. Johnsen and K. J. Lohmann, *Nature Rev. Neurosci.*, 2005, 6, 703-712.
10. C. V. Mora, M. Davison, J. M. Wild and M. M. Walker, *Nature*, 2004, 432, 508-511.
11. I. A. Solov'yov and W. Greiner, *Eur. Phys. J. D*, 2009, 51, 161-172.
12. I. A. Solov'yov and W. Greiner, *Phys. Rev. E*, 2009, 80, 041919.
13. I. A. Solov'yov and W. Greiner, *Biophys. J.*, 2007, 93, 1493-1509.
14. M. Zapka, D. Heyers, C. M. Hein, S. Engels, N. L. Schneider, J. Hans, S. Weiler, D. Dreyer, D. Kishkinev, J. M. Wild and H. Mouritsen, *Nature*, 2009, 461, 1274-1278.
15. K. Schulten, C. E. Swenberg and A. Weller, *Z. Phys. Chem.*, 1978, 111, 1-5.
16. U. E. Steiner and T. Ulrich, *Chem. Rev.*, 1989, 89, 51-147.
17. I. Chaves, R. Pokorny, M. Byrdin, N. Hoang, T. Ritz, K. Brettel, L. O. Essen, G. T. J. van der Horst, A. Batschauer and M. Ahmad, *Annu. Rev. Plant Biol.*, 2011, 62, 335-364.
18. Z. Schulten and K. Schulten, *J. Chem. Phys.*, 1977, 66, 4616-4634.
19. C. A. Dodson, P. J. Hore and M. I. Wallace, *Trends Biochem. Sci*, 2013, 38, 435-446.
20. T. Ritz, S. Adem and K. Schulten, *Biophys. J.*, 2000, 78, 707-718.
21. C. Niessner, S. Denzau, J. C. Gross, L. Peichl, H. J. Bischof, G. Fleissner, W. Wiltschko and R. Wiltschko, *Plos One*, 2011, 6, e20091.
22. H. Mouritsen, U. Janssen-Bienhold, M. Liedvogel, G. Feenders, J. Stalleicken, P. Dirks and R. Weiler, *Proc. Natl. Acad. Sci. U.S.A.*, 2004, 101, 14294-14299.
23. R. J. Gegear, A. Casselman, S. Waddell and S. M. Reppert, *Nature*, 2008, 454, 1014-1019.
24. W. Wiltschko, U. Munro, H. Ford and R. Wiltschko, *Nature*, 1993, 364, 525-527.
25. W. Wiltschko, U. Munro, H. Ford and R. Wiltschko, *Experientia*, 1993, 49, 167-170.
26. C. Niessner, S. Denzau, K. Stapput, M. Ahmad, L. Peichl, W. Wiltschko and R. Wiltschko, *J. R. Soc. Interface*, 2013, 10, 20130638.
27. T. Ritz, P. Thalau, J. B. Phillips, R. Wiltschko and W. Wiltschko, *Nature*, 2004, 429, 177-180.
28. S. Engels, N. L. Schneider, N. Lefeldt, C. M. Hein, M. Zapka, A. Michalik, D. Elbers, A. Kittel, P. J. Hore and H. Mouritsen, *Nature*, 2014, 509, 353-356.
29. T. Ritz, R. Wiltschko, P. J. Hore, C. T. Rodgers, K. Stapput, P. Thalau, C. R. Timmel and W. Wiltschko, *Biophys. J.*, 2009, 96, 3451-3457.
30. K. Maeda, A. J. Robinson, K. B. Henbest, H. J. Hogben, T. Biskup, M. Ahmad, E. Schleicher, S. Weber, C. R. Timmel and P. J. Hore, *Proc. Natl. Acad. Sci. U.S.A.*, 2012, 109, 4774-4779.
31. M. Liedvogel, K. Maeda, K. Henbest, E. Schleicher, T. Simon, C. R. Timmel, P. J. Hore and H. Mouritsen, *Plos One*, 2007, 2, e1106.
32. T. Biskup, E. Schleicher, A. Okafuji, G. Link, K. Hitomi, E. D. Getzoff and S. Weber, *Angew. Chem. Int. Ed.*, 2009, 48, 404-407.
33. B. Giovani, M. Byrdin, M. Ahmad and K. Brettel, *Nature Struct. Biol.*, 2003, 10, 489-490.
34. C. T. Rodgers and P. J. Hore, *Proc. Natl. Acad. Sci. U.S.A.*, 2009, 106, 353-360.

35. T. Langenbacher, D. Immeln, B. Dick and T. Kottke, *J. Am. Chem. Soc.*, 2009, 131, 14274-14280.
36. K. B. Henbest, K. Maeda, P. J. Hore, M. Joshi, A. Bacher, R. Bittl, S. Weber, C. R. Timmel and E. Schleicher, *Proc. Natl. Acad. Sci. U.S.A.*, 2008, 105, 14395-14399.
37. T. Biskup, K. Hitomi, E. D. Getzoff, S. Krapf, T. Koslowski, E. Schleicher and S. Weber, *Angew. Chem. Int. Ed.*, 2011, 50, 12647-12651.
38. T. Biskup, B. Paulus, A. Okafuji, K. Hitomi, E. D. Getzoff, S. Weber and E. Schleicher, *J. Biol. Chem.*, 2013, 288, 9249-9260.
39. A. A. Lee, J. C. S. Lau, H. J. Hogben, T. Biskup, D. R. Kattnig and P. J. Hore, *J. R. Soc. Interface*, 2014, 11, 20131063.
40. D. Immeln, A. Weigel, T. Kottke and J. L. P. Lustres, *J. Am. Chem. Soc.*, 2012, 134, 12536-12546.
41. H. J. Hogben, T. Biskup and P. J. Hore, *Phys. Rev. Lett.*, 2012, 109, 220501.
42. F. Cintolesi, T. Ritz, C. W. M. Kay, C. R. Timmel and P. J. Hore, *Chem. Phys.*, 2003, 294, 385-399.
43. I. A. Solov'yov, D. E. Chandler and K. Schulten, *Biophys. J.*, 2007, 92, 2711-2726.
44. C. R. Timmel, U. Till, B. Brocklehurst, K. A. McLauchlan and P. J. Hore, *Mol. Phys.*, 1998, 95, 71-89.
45. A. M. Stoneham, E. M. Gauger, K. Porfyrakis, S. C. Benjamin and B. W. Lovett, *Biophys. J.*, 2012, 102, 961-968.
46. B. Paulus, C. Bajzath, F. Melin, L. Heidinger, V. Kromm, C. Herkersdorf, U. Benz, L. Mann, P. Stehle, P. Hellwig, S. Weber and E. Schleicher, *FEBS J*, 2015, 282, 3175-3189.
47. I. A. Solov'yov and K. Schulten, *Biophys. J.*, 2009, 96, 4804-4813.
48. H. J. Hogben, O. Efimova, N. Wagner-Rundell, C. R. Timmel and P. J. Hore, *Chem. Phys. Lett.*, 2009, 480, 118-122.
49. K. Maeda, K. B. Henbest, F. Cintolesi, I. Kuprov, C. T. Rodgers, P. A. Liddell, D. Gust, C. R. Timmel and P. J. Hore, *Nature*, 2008, 453, 387-391.
50. X. L. Du, J. Wang, W. S. Pan, Q. J. Liu, X. J. Wang and W. J. Wu, *Photochem. Photobiol.*, 2014, 90, 989-996.
51. E. M. Gauger, E. Rieper, J. J. L. Morton, S. C. Benjamin and V. Vedral, *Phys. Rev. Lett.*, 2011, 106, 040503.
52. J. N. Bandyopadhyay, T. Paterek and D. Kaszlikowski, *Phys. Rev. Lett.*, 2012, 109, 110502.
53. E. M. Gauger and S. C. Benjamin, *Phys. Rev. Lett.*, 2013, 110, 178901.
54. J. M. Cai and M. B. Plenio, *Phys. Rev. Lett.*, 2013, 111, 230503.
55. J. M. Cai, F. Caruso and M. B. Plenio, *Phys. Rev. A*, 2012, 85, 040304.
56. B. M. Xu, J. Zou, J. G. Li and B. Shao, *Phys. Rev. E*, 2013, 88, 032703.
57. O. Efimova and P. J. Hore, *Biophys. J.*, 2008, 94, 1565-1574.
58. J. C. S. Lau, N. Wagner-Rundell, C. T. Rodgers, N. J. B. Green and P. J. Hore, *J. R. Soc. Interface*, 2010, 7, S257-S264.
59. I. A. Solov'yov, H. Mouritsen and K. Schulten, *Biophys. J.*, 2010, 99, 40-49.
60. E. Hill and T. Ritz, *J. R. Soc. Interface*, 2010, 7, S265-S271.
61. O. Efimova and P. J. Hore, *Mol. Phys.*, 2009, 107, 665-671.
62. J. M. Cai, G. G. Guerreschi and H. J. Briegel, *Phys. Rev. Lett.*, 2010, 104, 220502.
63. C. A. Brautigam, B. S. Smith, Z. Q. Ma, M. Palnitkar, D. R. Tomchick, M. Machius and J. Deisenhofer, *Proc. Natl. Acad. Sci. U.S.A.*, 2004, 101, 12142-12147.
64. G. Luedemann, I. A. Solov'yov, T. Kubar and M. Elstner, *J. Am. Chem. Soc.*, 2015, 137, 1147-1156.
65. I. A. Solov'yov, T. Domratcheva and K. Schulten, *Sci. Rep.*, 2014, 4, 3845.
66. I. A. Solov'yov, T. Domratcheva, A. R. M. Shahi and K. Schulten, *J. Am. Chem. Soc.*, 2012, 134, 18046-18052.
67. M. Ahmad, P. Galland, T. Ritz, R. Wiltschko and W. Wiltschko, *Planta*, 2007, 225, 615-624.

68. S. R. Harris, K. B. Henbest, K. Maeda, J. R. Pannell, C. R. Timmel, P. J. Hore and H. Okamoto, *J. R. Soc. Interface*, 2009, 6, 1193-1205.
69. C. X. Xu, S. F. Wei, Y. Lu, Y. X. Zhang, C. F. Chen and T. Song, *Bioelectromagnetics*, 2013, 34, 437-442.
70. I. A. Solov'yov, A. V. Yakubovich, P. V. Nikolaev, I. Volkovets and A. V. Solov'yov, *J. Comput. Chem.*, 2012, 33, 2412-2439.
71. J. C. Phillips, R. Braun, W. Wang, J. Gumbart, E. Tajkhorshid, E. Villa, C. Chipot, R. D. Skeel, L. Kale and K. Schulten, *J. Comput. Chem.*, 2005, 26, 1781-1802.
72. G. Luedemann, P. B. Woiczikowski, T. Kubar, M. Elstner and T. B. Steinbrecher, *J. Phys. Chem. B*, 2013, 117, 10769-10778.
73. H. D. Connor, B. E. Sturgeon, C. Mottley, H. J. Sipe and R. P. Mason, *J. Am. Chem. Soc.*, 2008, 130, 6381-6387.
74. R. Brosi, B. Illarionov, T. Mathes, M. Fischer, M. Joshi, A. Bacher, P. Hegemann, R. Bittl, S. Weber and E. Schleicher, *J. Am. Chem. Soc.*, 2010, 132, 8935-8944.
75. Y. T. Kao, C. Saxena, T. F. He, L. J. Guo, L. J. Wang, A. Sancar and D. P. Zhong, *J. Am. Chem. Soc.*, 2008, 130, 13132-13139.
76. J. D. Walsh and A. F. Miller, *Comp. Theor. Chem.*, 2003, 623, 185-195.
77. Z. B. Walters, *Phys. Rev. E*, 2014, 90, 042710.
78. K. V. Kavokin, *Bioelectromagnetics*, 2009, 30, 402-410.
79. M. J. Frisch, G. W. Trucks, H. B. Schlegel, G. E. Scuseria, M. A. Robb, J. R. Cheeseman, G. Scalmani, V. Barone, B. Mennucci, G. A. Petersson, H. Nakatsuji, M. Caricato, X. Li, H. P. Hratchian, A. F. Izmaylov, J. Bloino, G. Zheng, J. L. Sonnenberg, M. Hada, M. Ehara, K. Toyota, R. Fukuda, J. Hasegawa, M. Ishida, T. Nakajima, Y. Honda, O. Kitao, H. Nakai, T. Vreven, J. A. Montgomery Jr., J. E. Peralta, F. Ogliaro, M. J. Bearpark, J. Heyd, E. N. Brothers, K. N. Kudin, V. N. Staroverov, R. Kobayashi, J. Normand, K. Raghavachari, A. P. Rendell, J. C. Burant, S. S. Iyengar, J. Tomasi, M. Cossi, N. Rega, N. J. Millam, M. Klene, J. E. Knox, J. B. Cross, V. Bakken, C. Adamo, J. Jaramillo, R. Gomperts, R. E. Stratmann, O. Yazyev, A. J. Austin, R. Cammi, C. Pomelli, J. W. Ochterski, R. L. Martin, K. Morokuma, V. G. Zakrzewski, G. A. Voth, P. Salvador, J. J. Dannenberg, S. Dapprich, A. D. Daniels, Ö. Farkas, J. B. Foresman, J. V. Ortiz, J. Cioslowski and D. J. Fox, Gaussian, Inc., Wallingford, CT, USA, 2009.
80. K. Blum, *Density matrix theory and applications*, Springer, Heidelberg ; New York, 3rd edn., 2012.
81. H.-P. Breuer and F. Petruccione, *The theory of open quantum systems*, Oxford University Press, Oxford ; New York, 2002.
82. A. Papoulis and S. U. Pillai, *Probability, random variables, and stochastic processes*, McGraw-Hill, Boston, 4th edn., 2002.
83. C. T. Rodgers, S. A. Norman, K. B. Henbest, C. R. Timmel and P. J. Hore, *J. Am. Chem. Soc.*, 2007, 129, 6746-6755.
84. T. Y. Karogodina, I. G. Dranov, S. V. Sergeeva, D. V. Stass and U. E. Steiner, *ChemPhysChem*, 2011, 12, 1714-1728.
85. J. C. Weaver, T. E. Vaughan and R. D. Astumian, *Nature*, 2000, 405, 707-709.
86. T. Yoshii, M. Ahmad and C. Helfrich-Forster, *PLoS Biol.*, 2009, 7, 813-819.
87. R. J. Gegear, L. E. Foley, A. Casselman and S. M. Reppert, *Nature*, 2010, 463, 804-807
88. L. E. Foley, R. J. Gegear and S. M. Reppert, *Nature Comm.*, 2011, 2, 356.
89. G. Fedele, M. D. Edwards, S. Bhutani, J. M. Hares, M. Murbach, E. W. Green, S. Dissel, M. H. Hastings, E. Rosato and C. P. Kyriacou, *PLoS Genetics*, 2014, 10, e1004804.
90. G. Fedele, E. W. Green, E. Rosato and C. P. Kyriacou, *Nature Comm.*, 2014, 5, 4391.
91. O. Bazalova, M. Kvicalovac, T. Valkova, P. Slaby, P. Bartos, R. Netusil, K. Tomanova, P. Braeunig, H.-J. Lee, I. Sauman, M. Damulewicz, J. Provaznik, R. Pokorny, D. Dolezel and M. Vacha, *Proc. Natl. Acad. Sci. USA*, 2016, 113, 1660-1665.

TOC graphic:

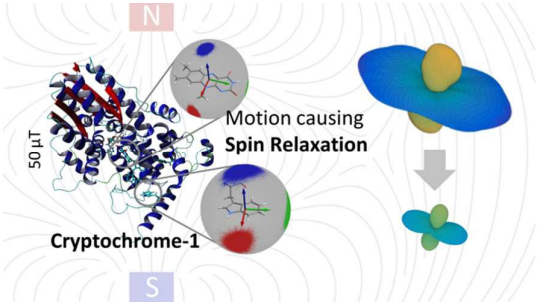

Table 1. Typical values of the secular spectral densities, $J(0)$, for different relaxation mechanisms.

Interaction	$J(0)^{-1}$ / μs
FAD – hyperfine terms*	
A_{zz}(N5)	0.066
A_{zz}(N5)/A_{zz}(N10)	0.20
A_{zz}(N10)	0.62
A_{zz}(N5)/A_{zz}(H6)	0.50
W – hyperfine terms	
A_{xx}(Hβ1)	0.075
A_{xx}(Hβ1)/A_{zz}(Hβ2)	0.16
A_{zz}(Hβ2)	0.33
A_{xx}(Hβ1)/A_{xx}(N1)	0.23
A_{xx}(Hβ1)/A_{yy}(H1)	0.26

* The axis designations of individual tensor elements correspond to the directions specified in Tables S1 to S3.

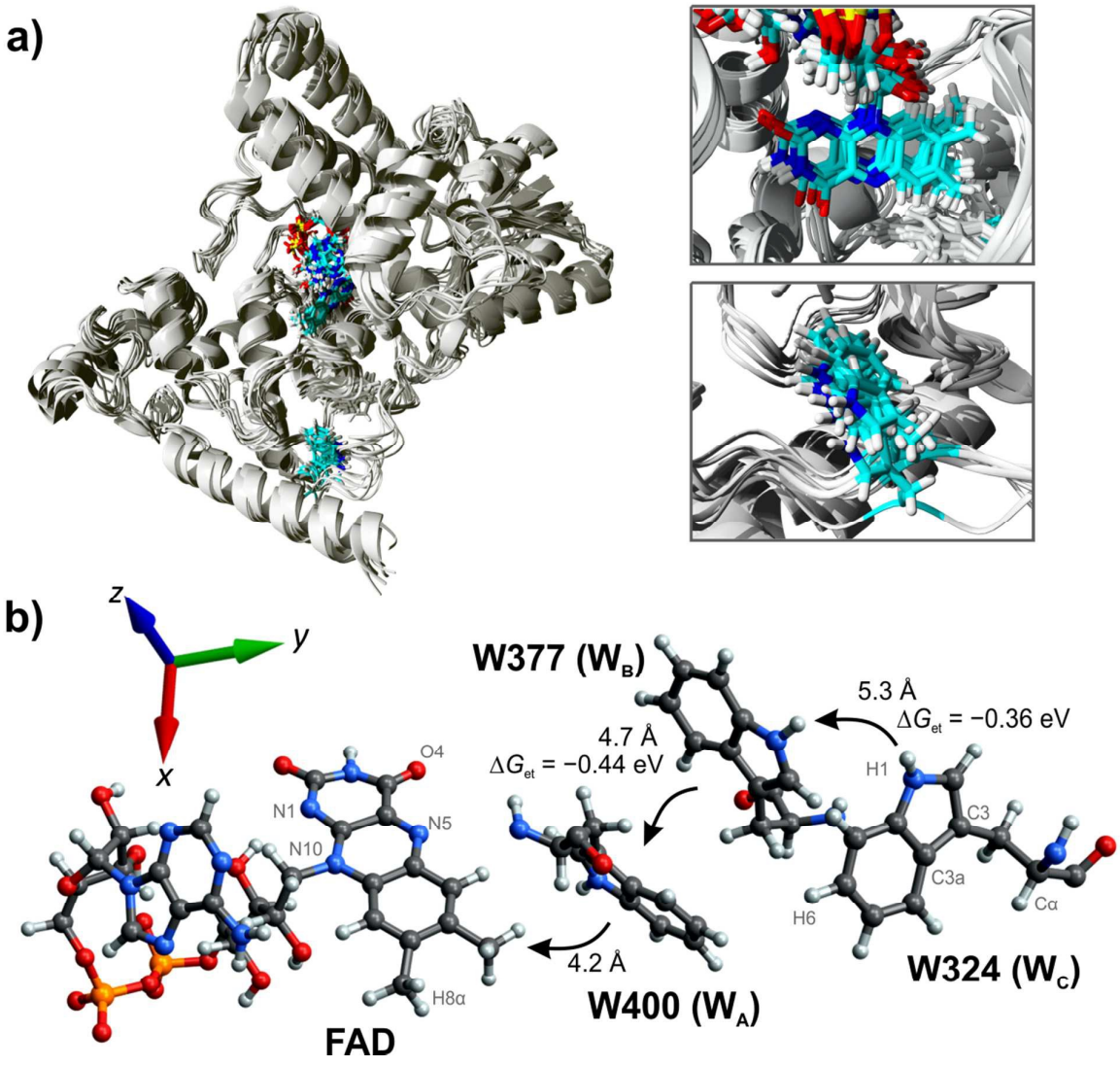

Figure 1. Structure of the photolyase homology domain of the charge-separated state of cryptochrome 1 from *A. thaliana* as determined by MD simulations starting from a modified crystal structure (PDB ID 1U3C) containing reduced FAD and oxidized W_C. (a) An illustration of the structural mobility by overlaying 7 MD-snapshots, separated by time intervals of 30 ns. The FAD cofactor and the tryptophan triad are shown in a stick representation (FAD and W_C in colour, W_A and W_B in grey). The images on the right provide close-ups of the cofactor and the terminal tryptophan. (b) The structure of FAD and the main electro-active residues arranged spatially as in the protein. The free energy changes of the radical pair intermediates resulting from successive electron transfers along the triad are indicated. These values, which reflect the solvent accessibility and stabilization of the respective tryptophan residue, are taken from Ref. 64. Also given are the smallest edge-to-edge distances of the aromatic rings of adjacent groups, obtained from the crystal structure. The protein coordinate system is shown in the top left corner. Figure S1 gives the atom numbering scheme.

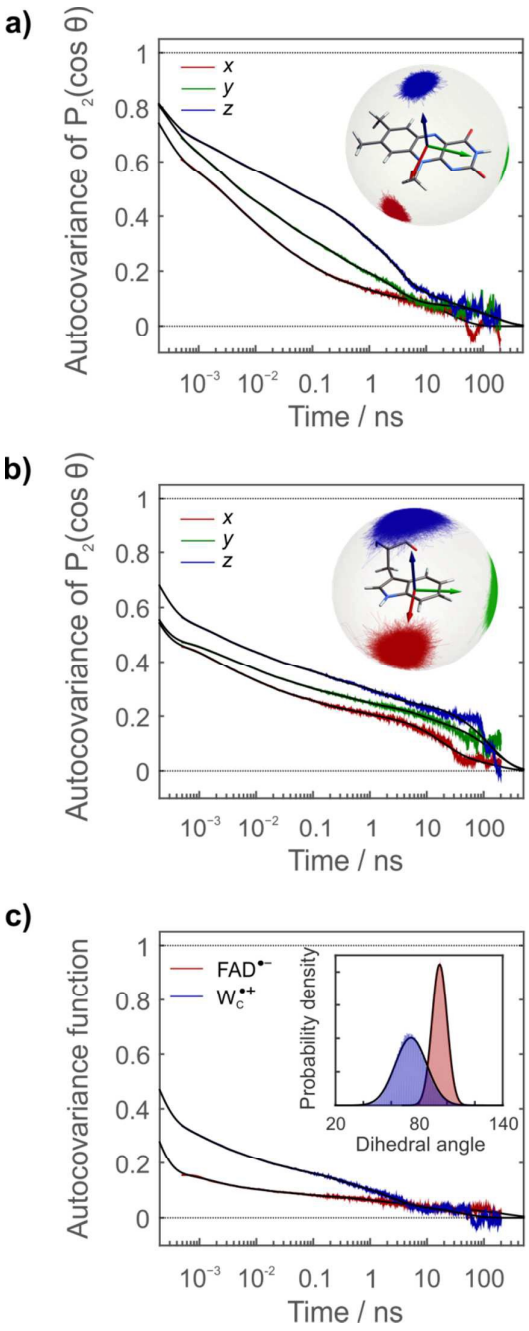

Figure 2. Characteristics of the relaxation-inducing motions of the radical centres in the protein. Parts (a) and (b) show, as insets, graphical representations of the orientational phase space sampled by small-angle fluctuations of the positions of the aromatic rings of $FAD^{\bullet-}$ (a) and $W_C^{\bullet+}$ (b). Also shown are the auto-covariance functions of $P_2(\cos\theta)$, with θ being the angle between the indicated molecular axis and its average orientation in the protein-fixed frame. For each radical, the molecular *z*-axis is perpendicular to the ring plane. (c) The torsional auto-covariance functions of the side-chain dihedral angles: C10a-N10-C1′-C2′ for $FAD^{\bullet-}$ and Cα-Cβ-C3-C3a for $W_C^{\bullet+}$; see Figure 1 and Figure S2. The inset shows the distribution functions of the two dihedral angles.

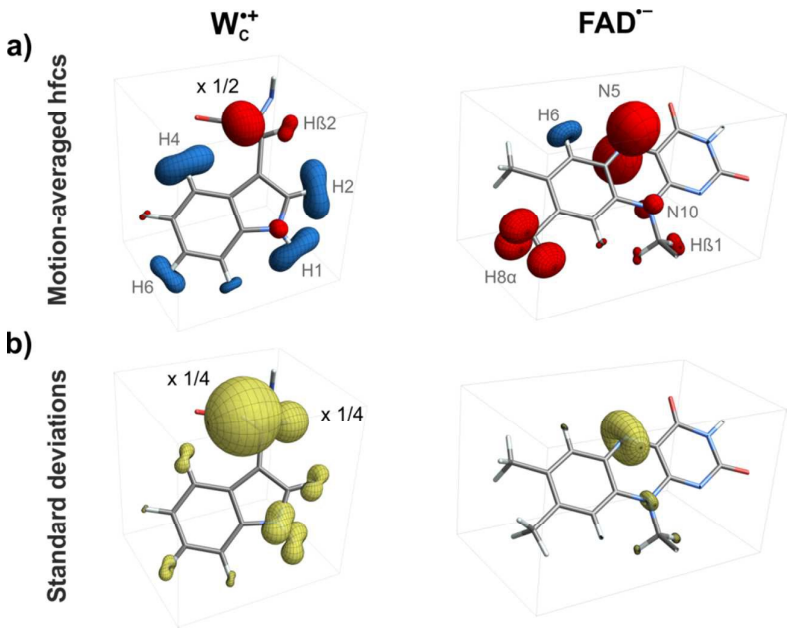

Figure 3. Graphical representation of the average hyperfine interactions of $FAD^{\bullet-}$ and $W_C^{\bullet+}$ (red and blue) and their standard deviations (yellow) over the course of 1.3 µs MD trajectories. (a) For any hyperfine tensor, **A**, and direction given by the unit vector, **r**, surfaces are drawn with distance $|\mathbf{r}^T\cdot\mathbf{A}\cdot\mathbf{r}|$ from the associated atom such that 1 Å corresponds to 18 MHz; red (blue) lobes indicate a positive (negative) value of $\mathbf{r}^T\cdot\mathbf{A}\cdot\mathbf{r}$. The hyperfine interactions of the methyl-protons on C8α in $FAD^{\bullet-}$ have been motionally averaged assuming free rotation about the C8α-C8 bond. (b) The standard deviations of the hyperfine interaction strengths $|\mathbf{r}^T\cdot\mathbf{A}\cdot\mathbf{r}|$ as obtained by propagation of variances are shown on the same scale as in (a). These values indicate the strength of the motion-induced fluctuations of the local hyperfine fields which, together with the temporal characteristics of the motion, determine the spin relaxation rates. Hence, efficient relaxation is expected to originate from N5 and N10 in $FAD^{\bullet-}$ and the β-methylene protons and several nuclei in the aromatic core of $W_C^{\bullet+}$, in particular, H1, N1 and H2.

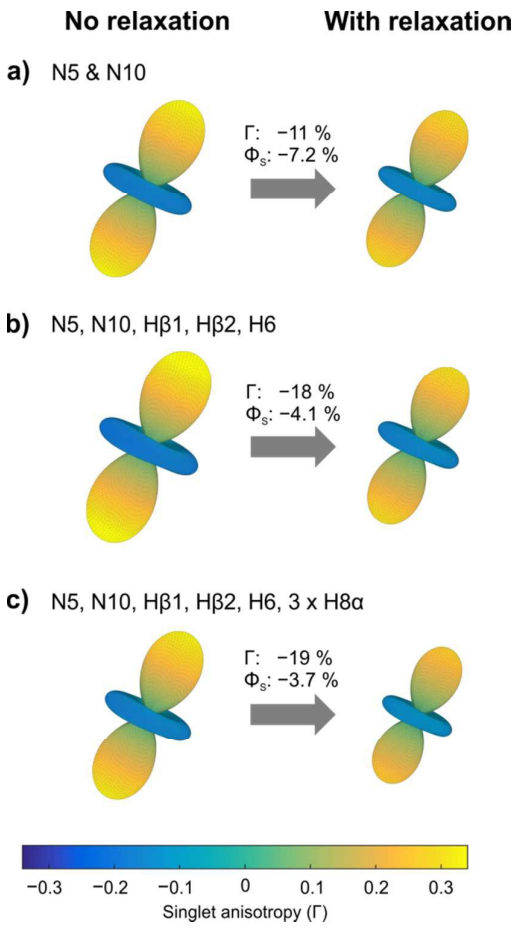

Figure 4. Spin relaxation effects on the singlet yield anisotropy of model [$FAD^{\bullet-}$ $Z^{\bullet}$] radical pairs arising from stochastic modulations of hyperfine interactions. Here, $Z^{\bullet}$ is a radical with no hyperfine interactions and no contribution to the spin relaxation. Each panel is labelled with the nuclei included in the calculation. The calculated singlet yield anisotropies are shown without (left) and with (right) spin relaxation. The distance in any direction from the centre of each pattern to the surface is proportional to $F_S - \bar{F}_S$ when the magnetic field has that direction. Yellow/blue regions correspond to reaction yields larger/smaller than the average. Cross-relaxation terms have been neglected; they gave rise to minor reductions in $F_S - \bar{F}_S$, indiscernible to the eye. The percentage changes of the mean singlet yield, $\bar{F}_S$, and the singlet anisotropy, Γ, are indicated. The remarkable aspect of this figure is the notable invariance of the singlet yield anisotropy when the size of the model spin system is extended. Additional simulation parameters: magnetic field = 50 μT, $k_S = k_T = 10^6$ s^{-1}, time-averaged hyperfine parameters as given in Table S1.

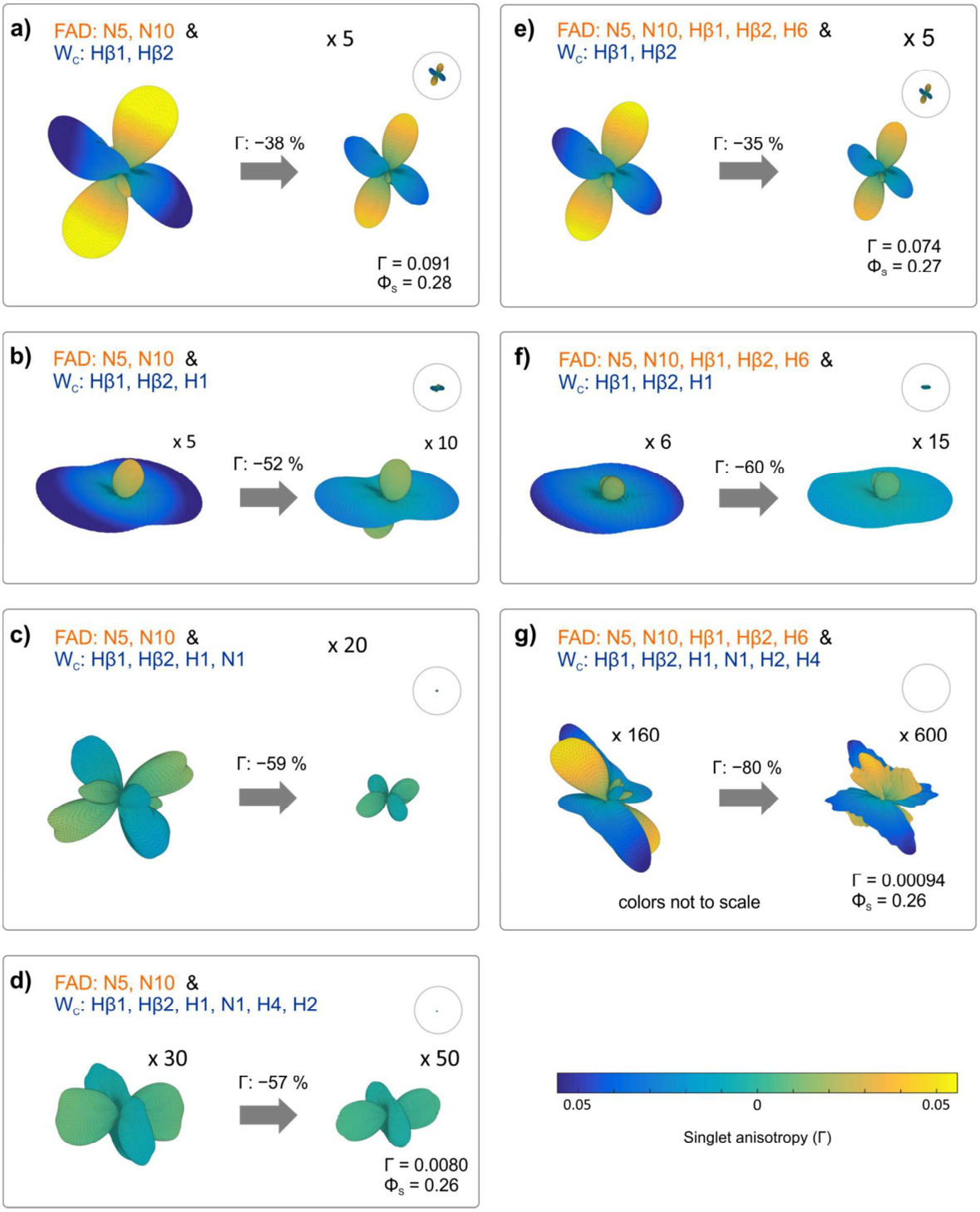

Figure 5. Effects of spin relaxation, on the singlet yield anisotropy of model [$FAD^{\bullet-}$ $W_C^{\bullet+}$] radical pairs, arising from stochastic modulations of hyperfine interactions. See Figure 4 for details. Each of the 7 panels is labelled by the nuclei included in the calculation, first in $FAD^{\bullet-}$ (orange labels), then in $W_C^{\bullet+}$ (blue labels). For clarity, the singlet yield anisotropies have been enlarged by the quoted scaling factors relative to the data for [$FAD^{\bullet-}$ $Z^{\bullet}$] in Figure 4. The circled inserts show the singlet yield anisotropy on the same scale as used in Figure 4. The colour bar, whose colour has been adjusted to

reflect the smaller values of Γ found in the presence of $W_C^{\cdot+}$, applies to all sub-plots with the exception of g), the largest spin system studied here. Additional simulation parameters: magnetic field = 50 μT, and $k_S = k_T = 10^6$ s^{-1}. The time-averaged hyperfine parameters are given in Tables S1 and S2. Cross-relaxation effects were excluded.

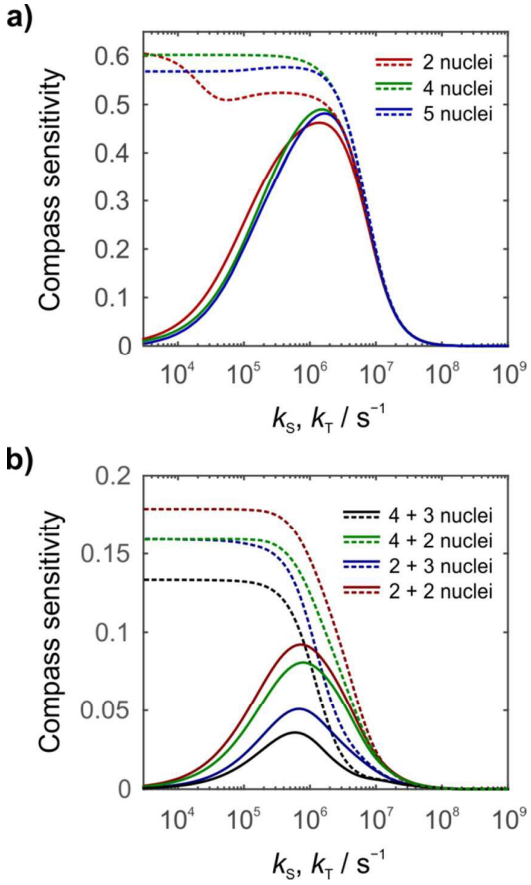

Figure 6. Dependence of the compass sensitivity (Γ) on the reaction rate constants for a) [$FAD^{\bullet-}$ $Z^{\bullet}$] and b) [$FAD^{\bullet-}$ $W_C^{\cdot+}$]. Solid and dashed lines are with and without motion-induced spin relaxation, respectively. The colours encode the spin system. For a) the first 2, 4, or 5 nuclei have been chosen from the set comprising N5, N10, Hβ1, Hβ2, and H6 (labels are defined in Figure 1 and Figure S1). For b), the nuclei with the strongest relaxation effects, i.e. the two nitrogen atoms and (optionally) the two β-protons in $FAD^{\bullet-}$ and the two β-protons and (optionally) H1 in $W_C^{\cdot+}$, have been considered. For all relaxing model systems, the maximum sensitivity is observed for lifetimes of approximately 1 µs. Additional parameters: magnetic field = 50 µT, $k_S = k_T$.